

# Smoothing splines on Riemannian manifolds, with applications to 3D shape space

Kwang-Rae Kim, Ian L. Dryden and Huiling Le,  
University of Nottingham, Nottingham, UK.

## Abstract

There has been increasing interest in statistical analysis of data lying in manifolds. This paper generalizes a smoothing spline fitting method to Riemannian manifold data based on the technique of unrolling and unwrapping originally proposed in [Jupp and Kent \(1987\)](#) for spherical data. In particular we develop such a fitting procedure for shapes of configurations in general  $m$ -dimensional Euclidean space, extending our previous work for two dimensional shapes. We show that parallel transport along a geodesic on Kendall shape space is linked to the solution of a homogeneous first-order differential equation, some of whose coefficients are implicitly defined functions. This finding enables us to approximate the procedure of unrolling and unwrapping by simultaneously solving such equations numerically, and so to find numerical solutions for smoothing splines fitted to higher dimensional shape data. This fitting method is applied to the analysis of simulated 3D shapes and to some dynamic 3D peptide data.

**Keywords:** cubic spline; geodesic; non-parametric regression; linear spline; peptide; tangent space; unrolling; unwrapping; wrapping.

## 1 Introduction

Analysis of temporal shape data has become increasingly important for applications in many fields, and a common definition is that the shape of an object is what is left after removing the effects of rotation, translation and re-scaling ([Kendall, 1984](#)). For an introduction to the statistical analysis of shape see [Dryden and Mardia \(2016\)](#); [Kendall et al. \(1999\)](#); [Patrangenaru and Ellingson \(2016\)](#) and [Srivastava and Klassen \(2016\)](#). Suppose that we are given time series of data which are measurements of a moving object. One may wish to find the overall trend or be interested in the behaviour of the object at unobserved times, including the explanation of how the shapes change between successive times or prediction in the future. For example, in the field of molecular biology, the study of dynamic proteins is of interest. However, currently there is very limited methodology available for fitting models for three-dimensional shape data which exhibit a large amount of variability.

The main difficulty in applying the classical statistical approach directly to analyse changes of shapes of configurations of  $k$  labelled landmarks over time lies in the fact that spaces of such shapes are curved, so that standard multivariate methods are not always appropriate. In the case where there is small variability in the set of shape data, one way to overcome this difficulty is to carry out the classical techniques on the projection of the data onto the Procrustes tangent space at their mean. For example one might wish to carry out multivariate linear regression, principal components analysis, or fit a spline through a series of shapes that change with time, e.g., see [Kent and Mardia \(2001\)](#) for Procrustes tangent projections, and [Kent et al. \(2001\)](#) and [Morris et al. \(1999\)](#) for some applications. The authors in [Kent et al. \(2001\)](#) applied such projections to two dimensional configuration data to construct models for the growth of shapes using roughness penalties, while the authors in [Morris et al. \(1999\)](#) combined such projections with principal component analysis to study the growth with age of the size-and-shapes of two dimensional profiles of human faces.

For data lying on a general Riemannian manifold and with large variability, geodesic based fitting approaches generalize the regression model for Euclidean data. Several different methods for fitting geodesics have been proposed. An early geodesic based model for detecting shape changes over time in Kendall shape space for planar configurations was proposed in [Le and Kume \(2000\)](#). [Fletcher et al. \(2004\)](#); [Fletcher \(2013\)](#) introduced principal geodesic analysis for data lying on a manifold, which uses the first principal component of the image of data under the inverse exponential map at their mean to determine the fitted geodesic for the given data. However, such a principal geodesic analysis may not always be appropriate for large variability as it assumes that the shape changes occur along a direction that passes through the mean. In [Kenobi et al. \(2010\)](#), the authors investigated a method for fitting minimal geodesics in Kendall shape space based on minimizing sums of squares of Procrustes distances. A more general method of principal geodesic analysis based on intrinsic methods of fitting geodesics to data on Riemannian manifolds was developed in [Huckemann and Ziezold \(2006\)](#) and [Huckemann et al. \(2010\)](#), and these methods are more widely applicable than principal geodesic analysis and provide an alternative definition of a mean.

Various methods for fitting regression models on manifolds with Euclidean covariates have been recently introduced, including regression on Riemannian symmetric spaces ([Cornea et al., 2017](#)), intrinsic polynomial regression ([Hinkle et al., 2014](#)), extrinsic local regression ([Lin et al., 2017](#)), global and local Fréchet regression ([Petersen and Müller, 2019](#)), and intrinsic and varying coefficient regression models for diffusion tensors ([Yuan et al., 2013](#); [Zhu et al., 2009](#)). It is also possible to generalize Euclidean smoothing spline fitting methods ([Green and Silverman, 1994](#)) to manifold-valued data. For example, [Su et al. \(2012\)](#) discussed the problem of fitting smoothing splines to data points on a Riemannian manifold measured over time using a Palais metric-based gradient method. To be able to implement this method in practice, complete knowledge of the geometric structure of manifolds is required. This is usually difficult for Kendall shape spaces of configurations lying in three dimensional Euclidean space.

Jupp and Kent (1987) proposed a method for fitting spherical smoothing splines to spherical data based on the techniques of unrolling and unwrapping onto an appropriate tangent space. The advantage of this approach is that, on the one hand, it retains certain geometric features of the data, such as lengths and angles, and on the other hand it does not require as much geometric knowledge as that in Su et al. (2012). The smoothing spline fitting method of Jupp and Kent (1987) was generalized to general linear groups in Pauley (2011), who denoted the curves ‘JK-cubics’ as solutions to a differential equation involving covariant derivatives. In addition, Pauley (2011) describes an alternative approach of Riemannian cubics on a manifold by solving more complicated Euler-Lagrange equations (which were also given by Jupp and Kent (1987) for a sphere), and also provides asymptotic analysis and links to a wider literature. Jupp and Kent (1987)’s unrolling and unwrapping smoothing spline method was also generalized to two dimensional shape data in Kume et al. (2007), using the result obtained in Le (2003) for unrolling procedures in general Kendall shape spaces. However, the study of shapes of configurations in three or more dimensions is much more complicated and, as noted in Kume et al. (2007), the method obtained there cannot be generalized to three dimensional shape data.

Our main contribution in this paper is that we give an explicit method for computing parallel transport for landmark shapes in at least three dimensions, and this is the first time that such a construction has been possible. Le (2003) discussed parallel transport in quotient spaces in general, and in particular her Theorem 1 gives three mathematical conditions which need to be satisfied for parallel transport in shape space. For landmarks shapes in  $m = 2$  dimensions explicit expressions are available which satisfy the conditions, and were utilized by Kume et al. (2007) for fitting smoothing splines. Le (2003)’s three conditions involve the unknown parallel transport vector  $V(s)$  and some unknown skew-symmetric matrices  $A(s)$  but no quantitative method of how to find such matrices and construct parallel transport in the general case. Although there was some discussion in special cases, no general method was given to construct a solution.

In our paper we give Proposition 3.1, with a proof, which enables us to find the  $A(s)$  and compute the parallel transport  $V(s)$  by numerically solving a system of homogeneous first-order ordinary differential equations (ODEs), some of whose coefficients are implicitly defined functions. A specific algorithm is outlined in the last couple of paragraphs in Section 3.2. So, for the first time, we are now able to compute the parallel transport for 3D shapes. In addition we implement the generalisation of Jupp and Kent (1987)’s smoothing splines using unrolling and unwrapping to 3D shape space. By solving the ODEs numerically we can approximate the procedure of unrolling and unwrapping, and hence obtain numerical solutions for smoothing splines fitted to three dimensional shape data. This is the first time that the unrolling and unwrapping procedure has been implemented for a non-homogenous quotient space as far as we are aware, building on the ideas of the previous  $m = 2$  homogeneous 2D shape space considered by Kume et al. (2007). Hence, our methodology has provided a large step up in generality to the very important practical case of analyzing

3D shape data.

This paper is organized as follows. In Section 2, we reformulate the procedures of unrolling and unwrapping, and then use them to define smoothing splines fitting on general manifolds. Since, as is clear from Section 2, the procedures of unrolling and unwrapping use the concept of so-called parallel transport, Section 3 provides some necessary basic geometry of shape space of labelled configurations in  $\mathbb{R}^m$  to develop parallel transport for general  $m$  for practical use. Numerical simulations and an application to real 3D peptide data are given in Section 4.

## 2 Smoothing splines on manifolds

### 2.1 Unrolling, unwrapping and wrapping

Recall that three of the main ingredients of the spline fitting technique used in Jupp and Kent (1987) and Kume et al. (2007) are respectively (i) unrolling a curve in the relevant space to the tangent space at its starting point; (ii) unwrapping points in the space at known times, with respect to a base path, onto the tangent space at the starting point of the path; and (iii) wrapping points onto a manifold, which is the reverse of unwrapping. Thus, to generalize spline fitting of Jupp and Kent (1987) and Kume et al. (2007) to general manifolds, we first reformulate these three procedures in a more general manifold setting.

Let  $M$  be a complete and connected Riemannian manifold with induced Riemannian distance  $d$  and denote by  $\tau_x(M)$  the tangent space to  $M$  at  $x \in M$ . Then, the exponential map on  $M$  at  $x$  can be expressed by

$$\exp_x : \tau_x(M) \mapsto M; \quad \exp_x(v) = \gamma(\|v\|),$$

where  $\gamma$  is the unit-speed geodesic such that  $\gamma(0) = x$  and  $\dot{\gamma}(0) = v/\|v\|$ . Thus, when there is a unique shortest unit-speed geodesic  $\gamma$  from  $x$  to  $x'$ , the inverse of the exponential map can be expressed as

$$\exp_x^{-1}(x') = d(x, x') \dot{\gamma}(0),$$

where  $d(x, x')$  is the induced Riemannian distance between  $x$  and  $x'$ .

Intuitive descriptions of the unrolling, unwrapping and wrapping procedures that we shall define can be found in Jupp and Kent (1987) for spherical data and Kume et al. (2007) for planar shape data. We paraphrase Kume et al. (2007) in following paragraph, but here it relates to a complete and connected Riemannian manifold  $M$ .

Consider a continuous and piecewise differentiable ( $C^1$ ) path  $\Gamma(t) \in [t_0, t_n]$ , in  $M$ . If we think of this path as being marked by wet ink, then its unrolling on to  $\mathcal{T} = \tau_{\Gamma(t_0)}(M)$ , the tangent space to  $M$  at the starting point ( $t_0$ ), is the trace  $\Gamma^\dagger$  left on  $\mathcal{T}$  after  $\mathcal{T}$  has been rolled without slipping or twisting along  $\Gamma(t)$  such that, at time  $t$ ,  $\mathcal{T}$  touches  $M$  at  $\Gamma(t)$ . The point, in  $\mathcal{T}$ , at which  $\mathcal{T}$  touches  $M$

at time  $t$  is  $\Gamma(t)^\dagger$ . The unwrapping at time  $t \in [t_0, t_n]$ , with respect to the base path  $\Gamma$ , of a point  $[w]$  in  $M$  is the point  $[w]^\dagger \in \mathcal{T}$  such that the tangent vector  $[w]^\dagger - \Gamma(t)^\dagger$  preserves the direction and distance of the point  $[w]$  in  $M$  when it is seen at time  $t$  by a person walking along at the same speed as that of the rolling of  $\mathcal{T}$  along  $\Gamma$ . In particular, the unrolling of a geodesic segment in  $M$  on to the tangent space at its initial shape is the straight-line segment, starting from the origin, that is determined by the tangent vector to the geodesic at its initial point and having the same length as the geodesic segment. The unrolling of a continuous piecewise shape geodesic segment on to the tangent space at its initial shape is a piecewise linear segment, starting from the origin, such that its first segment has the same length as the first geodesic segment and its direction is determined by the tangent vector to the first piece of the geodesic at its initial point, and the lengths of remaining segments are the same as the corresponding parts of the piecewise geodesic segment and the angles through which they turn are the same as those of the corresponding parts of the piecewise geodesic segment. Moreover, the unwrapping at time  $t$ , with respect to such a path  $\Gamma$  of a point  $[w]$  is the point  $[w]^\dagger \in \mathcal{T}$  such that the length of  $[w]^\dagger - \Gamma(t)^\dagger$  is the same as that of the geodesic from  $\Gamma(t)$  to  $[w]$  and the angle that  $[w]^\dagger - \Gamma(t)^\dagger$  makes with  $\Gamma^\dagger$  is the same as the angle that the geodesic from  $\Gamma(t)$  to  $[w]$  makes with the curve  $\Gamma$ . The piecewise geodesics in shape space, the piecewise linear paths in tangent space and the angles are displayed diagrammatically in Figure 1.

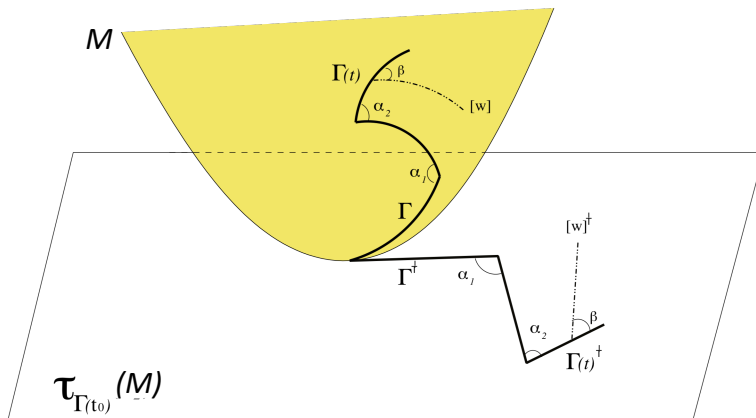


Figure 1: A diagrammatic view of unrolling, unwrapping and wrapping (adapted from [Kume et al., 2007](#)).

Formally, unrolling, unwrapping and wrapping are closely linked to the concept of parallel transport along a curve. The latter is a method of transporting tangent vectors along smooth curves in a manifold and, in some sense, provides a method of isometrically moving the local geometry of a manifold along curves. More precisely, suppose that  $\gamma(t)$ ,  $0 \leq t \leq t^*$  is a smooth curve in  $M$  and that

$v_0 \in \tau_{\gamma(0)}(M)$ , where  $t^* > 0$  is a fixed constant. Then, the parallel transport of  $v_0$  along  $\gamma$  is the extension of  $v_0$  to a vector field  $v$  on  $\gamma$  such that

$$\nabla_{\dot{\gamma}(t)} v(\gamma(t)) = 0, \quad v(\gamma(0)) = v_0,$$

where  $\nabla$  denotes the covariant derivative on  $M$ . This provides linear isomorphisms between the tangent spaces at points along the curve  $\gamma$ :

$$P_{\gamma(s)}^{\gamma(t)} : \tau_{\gamma(t)}(M) \rightarrow \tau_{\gamma(s)}(M).$$

This isomorphism is known as the (Levi-Civita) parallel transport map associated with the curve. Note that  $\left(P_{\gamma(s)}^{\gamma(t)}\right)^{-1} = P_{\gamma(t)}^{\gamma(s)}$ .

**Definition 2.1.** *In terms of the parallel transport  $P_{\gamma(s)}^{\gamma(t)}$  for a smooth curve  $\gamma$  in  $M$ :*

- the **unrolling** of  $\gamma$  onto  $\tau_{\gamma(0)}(M)$  is the curve  $\gamma^\dagger$  on  $\tau_{\gamma(0)}(M)$  such that  $\gamma^\dagger(0) = 0$  and

$$\frac{d\gamma^\dagger(t)}{dt} = P_{\gamma(0)}^{\gamma(t)}(\dot{\gamma}(t)), \quad 0 \leq t \leq t^*;$$

- the **unwrapping** at  $t \in [0, t^*]$ , with respect to  $\gamma$ , of a point  $x \in M$  into  $\tau_{\gamma(0)}(M)$  is the tangent vector at  $\gamma(0)$  obtained as follows: first map  $x$  to  $\tau_{\gamma(t)}(M)$  using  $\exp_{\gamma(t)}^{-1}$  to give  $\exp_{\gamma(t)}^{-1}(x)$ ; then parallel translate it along  $\gamma(t)$  back to  $\tau_{\gamma(0)}$  to give the tangent vector  $P_{\gamma(0)}^{\gamma(t)}(\exp_{\gamma(t)}^{-1}(x))$  at  $\gamma(0)$ ; finally, the unwrapping at  $t$  of  $x \in M$  into  $\tau_{\gamma(0)}(M)$  is the (Euclidean parallel) translation, within  $\tau_{\gamma(0)}(M)$ , of the tangent vector  $P_{\gamma(0)}^{\gamma(t)}(\exp_{\gamma(t)}^{-1}(x))$  to  $\gamma^\dagger(t)$ . In other words, the unwrapping at  $t$  of  $x \in M$  into  $\tau_{\gamma(0)}(M)$  is the sum of the two tangent vectors in  $\tau_{\gamma(0)}(M)$ :  $\gamma^\dagger(t)$  and the parallel transport of the tangent vector  $\exp_{\gamma(t)}^{-1}(x) \in \tau_{\gamma(t)}(M)$  along  $\gamma$  to  $\tau_{\gamma(0)}(M)$ , i.e. the unwrapping at  $t$  of  $x$ , with respect to  $\gamma$ , is

$$\gamma^\dagger(t) + P_{\gamma(0)}^{\gamma(t)}(\exp_{\gamma(t)}^{-1}(x));$$

- the **wrapping** at  $t$ , with respect to  $\gamma$ , of a tangent vector  $v \in \tau_{\gamma(0)}(M)$  back into  $M$  is the reverse of the unwrapping procedure.

In particular, if  $\gamma$  is a geodesic, then  $\gamma^\dagger$  is the linear segment of the same length as  $\gamma$  and in the same direction as the initial tangent vector of  $\gamma$ , that is, it is the linear segment from the origin of  $\tau_{\gamma(0)}(M)$  to  $\exp_{\gamma(0)}^{-1}(\gamma(t^*))$ .

## 2.2 Smoothing spline fitting on manifolds

Turning to smoothing splines on manifolds, we recall that, for  $v_0, v_1, \dots, v_n \in \mathbb{R}^d$  observed at times,  $t_0, t_1, \dots, t_n$  respectively, the cubic smoothing spline estimator for this dataset in  $\mathbb{R}^d$  is the function  $\widehat{f}_\lambda^\dagger : T \rightarrow \mathbb{R}^d$  that minimizes

$$\sum_{i=0}^n \left\| v_i - f_\lambda^\dagger(t_i) \right\|^2 + \lambda \int_T \left\| (f_\lambda^\dagger)''(t) \right\|^2 dt$$

among all  $\mathcal{C}^2$ -functions, where  $T = [t_0, t_n]$  and  $\lambda > 0$  denotes a smoothing parameter. This minimization problem can be solved on each component  $f^{\dagger(j)}$  of  $f^\dagger$  separately to reduce the  $d$ -dimensional minimization problem to  $d$  one dimensional ones, so that

$$\widehat{f}_\lambda^{\dagger(j)} = \operatorname{argmin}_{f_\lambda^{\dagger(j)}} \sum_{i=0}^n \left\{ v_i^{(j)} - f_\lambda^{\dagger(j)}(t_i) \right\}^2 + \lambda \int_T \left\{ \left( f_\lambda^{\dagger(j)} \right)''(t) \right\}^2 dt, \quad (1)$$

for  $j = 1, \dots, d$ . The solution to such a minimization problem is a cubic spline with knots at the unique values of  $v_i$ , while the smoothing parameter  $\lambda$  controls the trade-off of the model complexity. When  $\lambda$  tends to zero,  $\widehat{f}_\lambda^\dagger$  becomes any function interpolating the data points. On the other hand,  $\widehat{f}_\lambda^\dagger$  becomes a classical simple linear regression line when  $\lambda$  tends to infinity. The integrated squared second derivative penalty function leads to the cubic smoothing spline which often works well in practice. Alternatively using  $m \geq 2$  order derivatives in the penalty leads to a spline of order  $2m - 1$ .

Penalties with other functional forms could also be used and the knots do not need to coincide with the data points. For example we also consider a total variation norm penalty ( $TV(g) = \int_T |g'| dt$ ) on the first derivative of each component, i.e.

$$\widehat{f}_{L,\lambda}^{\dagger(j)} = \operatorname{argmin}_{f_\lambda^{\dagger(j)}} \sum_{i=0}^n \left\{ v_i^{(j)} - f_\lambda^{\dagger(j)}(t_i) \right\}^2 + \lambda \int_T \left| \left( f_\lambda^{\dagger(j)} \right)'(t) \right| dt, \quad (2)$$

for  $j = 1, \dots, d$ . The solution is a linear spline for each component, which consists of a piecewise linear function with possible jumps in the slope at each knot (Koenker and Mizera, 2004). We consider such linear splines with a small number of equally spaced knots (not necessarily at data points) and small  $\lambda$  so that there is a change in slope at each of the knots.

In a similar fashion to that in Jupp and Kent (1987) and Kume et al. (2007), we use the concept of unrolling and unwrapping to define  $M$ -valued smooth splines as follows.

**Definition 2.2.** For a given dataset  $\mathcal{D} = \{x_j : 0 \leq j \leq n\}$  in  $M$ , where  $x_j$  is observed at time  $t_j$ , and smoothing parameter  $\lambda$ , we define **the  $M$ -valued smoothing spline fitted to  $\mathcal{D}$  with parameter  $\lambda$**  to be the  $\mathcal{C}^2$ -function

$$f(\cdot, \lambda) : [t_0, t_n] \rightarrow M$$

such that its unrolling  $f^\dagger$  onto  $\tau_{f(t_0, \lambda)}(M)$  is the cubic smoothing spline fitted to the data  $\mathcal{D}^\dagger$  obtained by unwrapping  $\mathcal{D}$  at times  $t_j$ , with respect to  $f(\cdot, \lambda)$ , into  $\tau_{f(t_0, \lambda)}(M)$ .

To find the smoothing spline fitted to a given dataset  $\mathcal{D}$ , the iterative scheme for approximation given in [Jupp and Kent \(1987\)](#) can be applied to general manifolds: take the piecewise geodesic passing through the data points as the initial curve  $f_0$ ; at each step  $\ell \geq 0$ , unwrap  $\mathcal{D}$  with respect to  $f_\ell$  to get  $\mathcal{D}_\ell^\dagger$  in  $\tau_{f_\ell(t_0)}(M)$ ; fit a Euclidean smoothing spline  $f_{\ell+1}^\dagger$  to  $\mathcal{D}_\ell^\dagger$  in  $\tau_{f_\ell(t_0)}(M)$ ; then the curve  $f_{\ell+1}$  is defined to be the wrapped path, with respect to  $f_\ell$ , of  $f_{\ell+1}^\dagger$  in  $M$ . The iterative procedure stops when  $f_\ell$  and  $f_{\ell+1}$  are sufficiently close.

In such an iterative scheme, smooth curves are approximated by piecewise geodesics. Thus, for the implementation in practice, it is sufficient to restrict ourselves to the procedures of unrolling a piecewise geodesic and of unwrapping and wrapping with respect to a piecewise geodesic.

**Proposition 2.1.** *For a given curve  $\gamma(t)$ ,  $t_0 \leq t \leq t_n$ , on  $M$ , which is a geodesic between  $t_i$  and  $t_{i+1}$ , where  $t_0 < t_1 < \dots < t_n$ , the above unrolling, unwrapping and wrapping procedures along  $\gamma$  can be formulated as follows.*

- The unrolling of  $\gamma$  onto  $\tau_{\gamma(t_0)}(M)$  is the piecewise linear segment in the tangent space  $\tau_{\gamma(t_0)}(M)$  joining the following successive points:

$$\gamma(t_i)^\dagger = \begin{cases} 0 & i = 0 \\ \gamma(t_{i-1})^\dagger + P_{\gamma(t_0)}^{\gamma(t_1)} \circ P_{\gamma(t_1)}^{\gamma(t_2)} \circ \dots \circ P_{\gamma(t_{i-2})}^{\gamma(t_{i-1})} \left( \exp_{\gamma(t_{i-1})}^{-1}(\gamma(t_i)) \right) & 1 \leq i \leq n. \end{cases}$$

Note that

$$\gamma^\dagger(t) = \gamma(t_j)^\dagger + \frac{t - t_j}{t_{j+1} - t_j} \{ \gamma(t_{j+1})^\dagger - \gamma(t_j)^\dagger \} \quad \text{for } t_i < t \leq t_{j+1}.$$

- The unwrapping at time  $t$  of  $x \in M$ , with respect to  $\gamma$ , into  $\tau_{\gamma(t_0)}(M)$  is the tangent vector  $x_t^\dagger \in \tau_{\gamma(t_0)}(M)$  given by

$$x_t^\dagger = \begin{cases} \exp_{\gamma(t_0)}^{-1}(x) & \text{if } t = t_0 \\ \gamma(t)^\dagger + P_{\gamma(t_0)}^{\gamma(t_1)} \circ P_{\gamma(t_1)}^{\gamma(t_2)} \circ \dots \circ P_{\gamma(t_{j-1})}^{\gamma(t_j)} \circ P_{\gamma(t_j)}^{\gamma(t)} \left( \exp_{\gamma(t)}^{-1}(x) \right) & \text{if } t_j < t \leq t_{j+1}, \end{cases}$$

as long as  $x$  is not in the cut locus of  $\gamma(t)$ .

- The wrapping at time  $t \in [t_0, t_n]$ , along  $\gamma$ , of a tangent vector  $v \in \tau_{\gamma(t_0)}(M)$  back into  $M$  is the point  $x_t \in M$  given by

$$x_t = \exp_{\gamma(t)}(v_t),$$

where  $v_t$  is the tangent vector in  $\tau_{\gamma(t)}(M)$  specified by

$$v_t = \begin{cases} v & \text{if } t = t_0 \\ P_{\gamma(t)}^{\gamma(t_j)} \circ P_{\gamma(t_j)}^{\gamma(t_{j-1})} \circ \dots \circ P_{\gamma(t_1)}^{\gamma(t_0)} (v - \gamma(t)^\dagger) & \text{if } t_j < t \leq t_{j+1}. \end{cases}$$

It is clear that, to be able to carry out the unrolling, unwrapping and wrapping procedures in practice, the crucial steps are to find the expressions for the exponential map, as well as its inverse, and for the parallel transport along a geodesic.

**Example:** The expressions for unrolling, unwrapping and wrapping are known in the case of the unit sphere  $S^d$ :

- a unit speed geodesic starting from  $x \in S^d$  takes the form

$$\gamma(t) = x \cos(t) + v \sin(t), \quad (3)$$

where  $v \in \mathbb{R}^{d+1}$  such that  $\|v\| = 1$  and  $\langle x, v \rangle = 0$ ;

- the exponential map at  $x$  has the expression

$$\exp_x(v) = x \cos(\|v\|) + \frac{v}{\|v\|} \sin(\|v\|) \quad (4)$$

for any  $v \in \mathbb{R}^{d+1} \setminus \{0\}$  such that  $\langle x, v \rangle = 0$ ;

- the inverse exponential at  $x$  is given by

$$\exp_x^{-1}(x') = \frac{x' - \langle x, x' \rangle x}{\|x' - \langle x, x' \rangle x\|} \arccos(\langle x, x' \rangle)$$

for all  $x' \in S^d \setminus \{-x\}$ ;

- the parallel transport of the tangent vector  $w \in \tau_{\gamma(t_0)}(S^d)$  along the geodesic  $\gamma$  defined by (3) is the vector field  $w(t)$  along  $\gamma(t)$  given by

$$w(t) = w - \langle w, v \rangle (v - \dot{\gamma}(t)),$$

where  $v = \dot{\gamma}(0)$ , as  $w(t) \in \tau_{\gamma(t)}(S^d)$  and as the covariant derivative of  $w(t)$  along  $\gamma$  is  $\nabla_{\dot{\gamma}(t)} w(t) = \dot{w}(t) - \langle \dot{w}(t), \gamma(t) \rangle \gamma(t)$ .

### 3 Smoothing splines in shape space

The method in the previous section provides a general framework for fitting smooth splines on manifolds. Unfortunately, due to their non-trivial geometric

structure, the direct implementation on the Kendall shape spaces for configurations in  $\mathbb{R}^m$  ( $m \geq 3$ ) of the exponential map and, in particular, of the parallel transport turns out to be challenging. This in turn makes the practical implementation of the spline fitting idea proposed in the previous section difficult. One possible way to overcome this difficulty is to explore the fact that Kendall shape spaces are the quotient spaces of Euclidean spheres and to use the much simpler structure of spheres, as has previously been done by many in various different statistical investigations in shape analysis. For example, Le (2003) obtained an equivalent, qualitative description of the parallel transport on shape spaces via the pre-shape sphere. In the case of shapes of configurations in  $\mathbb{R}^2$ , this description leads successfully to a closed expression for such an equivalent notion on the pre-shape sphere, which has then been used for statistical analysis of shape in Kume et al. (2007). Unfortunately, as pointed out in Le (2003), such a closed expression is generally unavailable on the shape space of configurations in  $\mathbb{R}^m$  for  $m \geq 3$ . In this section, we summarize the facts required for the exponential maps on the shape space of labelled configurations in  $\mathbb{R}^m$  and develop the result in Le (2003) further for general  $m$  to the extent that it is usable for practical purposes.

### 3.1 Shape space, its tangent space and shape geodesics

Recall that, for a configuration in  $\mathbb{R}^m$  with  $k (> m)$  labelled landmarks, its pre-shape is what is left after the effects of translation and scaling are removed and that this pre-shape can be represented by an  $m \times (k - 1)$  matrix  $X$  with  $\|X\|^2 = \text{tr}(XX^\top) = 1$ . The space  $\mathcal{S}_m^k$  of such pre-shapes is known as the pre-shape space of configurations of  $k$  labelled landmarks in  $\mathbb{R}^m$  and is the unit sphere of dimension  $m(k - 1) - 1$ , i.e.  $\mathcal{S}_m^k = S^{m(k-1)-1}$ . The Kendall shape space  $\Sigma_m^k$  of configurations with  $k$  labelled landmarks in  $\mathbb{R}^m$  is then the quotient space of  $\mathcal{S}_m^k$  by the rotation group  $SO(m)$  acting on the left (cf. Dryden and Mardia (2016) and Kendall et al. (1999)). We shall use  $[X]$  to denote the shape of the pre-shape  $X$ .

Writing  $M(m, k - 1)$  for the space of  $m \times (k - 1)$  real matrices, then the tangent space to  $\mathcal{S}_m^k$  at  $X \in \mathcal{S}_m^k$  is

$$\tau_X(\mathcal{S}_m^k) = \{V \in M(m, k - 1) \mid \text{tr}(XV^\top) = 0\}.$$

The horizontal subspace, which is the same as the Procrustean tangent space, of  $\tau_X(\mathcal{S}_m^k)$ , with respect to the quotient map from  $\mathcal{S}_m^k$  to  $\Sigma_m^k$ , can be expressed as

$$\mathcal{H}_X(\mathcal{S}_m^k) = \{V \in M(m, k - 1) \mid \text{tr}(XV^\top) = 0, XV^\top \text{ is symmetric}\}.$$

The horizontal subspace  $\mathcal{H}_X(\mathcal{S}_m^k)$  is isometric to the tangent space  $\tau_{[X]}(\Sigma_m^k)$  to  $\Sigma_m^k$  at the shape  $[X]$  of  $X$ , and this gives a useful isometric representation of the tangent space of  $\Sigma_m^k$  at  $[X]$  for the statistical analysis of shapes (cf. Kendall et al., 1999). Note that the shape of a configuration becomes singular when the rank of the configuration matrix is less than  $m - 1$ . To apply the results

and methodology of the previous section, we have in fact implicitly restricted ourselves to situations where shapes are non-singular as is the case for most applications. We shall continue to make this restriction. Since the set of singular shapes has a high co-dimension and geodesics between any two non-singular shapes never pass through singular shapes, this restriction is relatively mild.

A unit-speed geodesic  $\gamma$  in the shape space starting from  $[X]$  can be isometrically represented by a so-called horizontal geodesic in  $\mathcal{S}_m^k$  of the form

$$\Gamma(s) = X \cos s + V \sin s, \quad s \in [0, \pi/2),$$

where  $V \in \mathcal{H}_X(\mathcal{S}_m^k)$  and  $\|V\| = 1$ . The path  $\Gamma$  is usually referred to as the horizontal lift of  $\gamma$ . To obtain a representation of a shortest geodesic between two shapes  $[X_1]$  and  $[X_2]$ , we take the two pre-shapes  $X_1$  and  $X_2$  of  $[X_1]$  and  $[X_2]$  respectively such that  $X_1 X_2^\top$  is symmetric and all its eigenvalues are non-negative except possibly for  $\lambda_m$ , the smallest one, where  $\text{sign}(\lambda_m) = \text{sign}(\det(X_1 X_2^\top))$ . Then, a unit-speed shortest geodesic from  $[X_1]$  to  $[X_2]$  can be isometrically represented by the horizontal geodesic from  $X_1$  to  $X_2$ :

$$\Gamma(s) = X_1 \cos s + V_{X_1, X_2} \sin s, \quad s \in [0, s_0], \quad (5)$$

where

$$V_{X_1, X_2} = \frac{1}{\sin s_0} \{X_2 - X_1 \cos s_0\} \in \mathcal{H}_{X_1}$$

and  $s_0 = \rho([X_1], [X_2])$  is the Riemannian shape distance between  $[X_1]$  and  $[X_2]$ . Note that  $\|V_{X_1, X_2}\| = 1$ .

Thus, it follows from the expression (5) for the horizontal geodesic from  $X_1$  to  $X_2$  that, if there is a unique geodesic between  $[X_1]$  and  $[X_2]$ , the inverse exponential map  $\exp_{[X_1]}^{-1}([X_2])$  on the shape space  $\Sigma_m^k$  can be isometrically represented by its horizontal lift on  $\mathcal{S}_m^k$  given by

$$\exp_{X_1}^{-1}(X_2) = s_0 V_{X_1, X_2}. \quad (6)$$

### 3.2 Parallel transport

Turning to parallel transport, it is shown in Le (2003) that, along a horizontal geodesic  $\Gamma(s)$  in  $\mathcal{S}_m^k$ , a vector field  $V(s)$  is horizontal and its projection to  $\tau_{[\Gamma(s)]}(\Sigma_m^k)$  is the parallel transport, along the shape geodesic  $[\Gamma(s)]$ , of the projection of  $V(0)$  to  $\tau_{[\Gamma(0)]}(\Sigma_m^k)$  if and only if  $V(s)$  satisfies the following three conditions:

$$\text{tr}(V(s) \Gamma(s)^\top) = 0 \quad (7)$$

$$V(s) \Gamma(s)^\top = \Gamma(s) V(s)^\top \quad (8)$$

$$\dot{V}(s) - \text{tr}(\Gamma(s) \dot{V}(s)^\top) \Gamma(s) = A(s) \Gamma(s) \quad \text{for some } A(s) \text{ such} \quad (9)$$

that  $A(s) = -A(s)^\top$ .

Thus, the solution  $V(s)$  to (7), (8) and (9) provides an isometric representation, on  $\mathcal{S}_m^k$ , of the parallel transport  $P_{[\Gamma(s_0)]}^{[\Gamma(0)]}$  along  $[\Gamma(s)]$ ,  $0 \leq s \leq s_0$ :

$$\Psi_{\Gamma(s_0)}^{\Gamma(0)} : V(0) \mapsto V(s_0). \quad (10)$$

The usefulness of this result for practical implementation lies crucially in obtaining a more quantitative description of the skew-symmetric matrix  $A(s)$  in (9), which we derive with the following result.

**Proposition 3.1.** *Let  $\Gamma(s)$ ,  $0 \leq s \leq s_0$ , be a given horizontal  $\mathcal{C}^1$ -curve in  $\mathcal{S}_m^k$  and  $V$  be a given horizontal tangent vector in  $\tau_{\Gamma(0)}(\mathcal{S}_m^k)$ . Assume that the rank of  $\Gamma(s)$  is at least  $m - 1$ , except for at most finitely many  $s$ . Then, the vector field  $V(s)$  along  $\Gamma(s)$  is horizontal and the projection of  $V(s)$  to  $\tau_{[\Gamma(s)]}(\Sigma_m^k)$  is the parallel transport, along the shape curve  $[\Gamma(s)]$ , of the projection of  $V$  to  $\tau_{[\Gamma(0)]}(\Sigma_m^k)$  if and only if  $V(s)$  is the solution of*

$$\begin{aligned} \dot{V}(s) &= -\text{tr}(\dot{\Gamma}(s) V(s)^\top) \Gamma(s) + A(s) \Gamma(s), & s \in [0, s_0], \\ V(0) &= V, \end{aligned} \quad (11)$$

where  $A(s)$  is skew-symmetric and is the unique solution to

$$A(s) \Gamma(s) \Gamma(s)^\top + \Gamma(s) \Gamma(s)^\top A(s) = \dot{\Gamma}(s) V(s)^\top - V(s) \dot{\Gamma}(s)^\top. \quad (12)$$

*Proof.* Note first that  $V \in \mathcal{H}_{\Gamma(0)}(\mathcal{S}_m^k)$  implies that  $\text{tr}(V\Gamma(0)^\top) = 0$  and  $V\Gamma(0)^\top$  is a symmetric matrix.

Assume that  $V(s)$  satisfies (7), (8) and (9). Since  $\text{tr}(V(0)\Gamma(0)^\top) = 0$ , condition (7) holds for all  $s \in [0, s_0]$  if and only if

$$\text{tr}(\dot{V}(s)\Gamma(s)^\top) + \text{tr}(V(s)\dot{\Gamma}(s)^\top) = 0, \quad s \in [0, s_0]. \quad (13)$$

Thus, under conditions (7) and (9),  $V(s)$  satisfies (11) for some skew-symmetric matrix  $A(s)$ . Since  $V(0)\Gamma(0)^\top = \Gamma(0)V(0)^\top$ , condition (8) holds if and only if

$$\dot{V}(s)\Gamma(s)^\top + V(s)\dot{\Gamma}(s)^\top = \dot{\Gamma}(s)V(s)^\top + \Gamma(s)\dot{V}(s)^\top,$$

which is equivalent to

$$\dot{V}(s)\Gamma(s)^\top - \Gamma(s)\dot{V}(s)^\top = \dot{\Gamma}(s)V(s)^\top - V(s)\dot{\Gamma}(s)^\top. \quad (14)$$

Hence, if (9) holds for some  $A(s)$  such that  $A(s) = -A(s)^\top$ ,  $A(s)$  must satisfy

$$\dot{V}(s)\Gamma(s)^\top - \Gamma(s)\dot{V}(s)^\top = A(s)\Gamma(s)\Gamma(s)^\top + \Gamma(s)\Gamma(s)^\top A(s).$$

Thus, conditions (8) and (9) together imply that  $A(s)$  must satisfy (12).

The uniqueness of the solution to (12) follows from the fact that, for a given  $m \times m$  symmetric non-negative definite matrix  $S = R\Lambda R^\top$  of rank at

least  $m - 1$ , where  $R \in \mathbf{O}(m)$  and  $\Lambda = \text{diag}\{\lambda_1, \dots, \lambda_m\}$ , and a given skew-symmetric matrix  $B$ , there is a unique skew-symmetric matrix  $A$  satisfying the equation  $AS + SA = B$ . To see the latter, write  $\tilde{A} = (\tilde{a}_{ij}) = R^\top AR$  and  $\tilde{B} = (\tilde{b}_{ij}) = R^\top BR$ . Then,  $AS + SA = B$  if and only if  $\tilde{A}\Lambda + \Lambda\tilde{A} = \tilde{B}$ , which is if and only if  $\lambda_i\tilde{a}_{ij} + \lambda_j\tilde{a}_{ji} = \tilde{b}_{ij}$  for  $i < j$ , i.e. if and only if  $\tilde{a}_{ij} = \tilde{b}_{ij}/(\lambda_i + \lambda_j)$ .

On the other hand, if  $V(s)$  is the solution to (11) with  $A(s)$  being determined by (12), then  $V(s)$  satisfies (14) and so (8) holds. However,  $\text{tr}(A(s)\Gamma(s)\Gamma(s)^\top) = \text{tr}(\Gamma(s)\Gamma(s)^\top A(s))$ , so that condition (12) implies that we must have

$$\text{tr}(A(s)\Gamma(s)\Gamma(s)^\top) = 0.$$

This, together with (14), shows that  $V(s)$  also satisfies (13). Hence, both (7) and (9) hold.  $\square$

Note that  $V(s)$  given in Proposition 3.1 is generally not the parallel transport of  $V$  along  $\Gamma(s)$  in  $\mathcal{S}_m^k$ . The reason for this is that, in terms of the covariant derivative  $\nabla$  on  $\mathcal{S}_m^k$ , one requires  $\nabla_{\dot{\Gamma}(s)}V(s) = 0$  for  $V(s)$  to be the parallel transport of  $V(0)$  along  $\Gamma$  in  $\mathcal{S}_m^k$ , while one only needs  $\nabla_{\dot{\Gamma}(s)}V(s)$  to be orthogonal to the horizontal subspace  $\mathcal{H}_{\Gamma(s)}(\mathcal{S}_m^k)$ , as explained in Le (2003), for the projection of  $V(s)$  to be the parallel transport along  $[\Gamma(s)]$  of the projection of  $V(0)$ . The latter is the one that we require.

To apply the above results to the parallel transport of the projection of  $V(s_0)$  along  $[\Gamma(s)]$ ,  $0 \leq s \leq s_0$ , back to  $\tau_{[\Gamma(0)]}(\Sigma_m^k)$  that we require for the unrolling and unwrapping procedures, we re-parametrize the curve  $\Gamma(s)$  and the vector field  $V(s)$  to  $\tilde{\Gamma}(s) = \Gamma(s_0 - s)$  and  $\tilde{V}(s) = V(s_0 - s)$ , say, respectively. With this modification in mind, the result of Proposition 3.1 would appear to provide a numerical method to approximate  $\Psi_{\Gamma(0)}^{\Gamma(s_0)}$  in the usual way: with step size  $\delta = s_0/\ell$ ,  $V^*(\ell\delta) = V(s_0)$ ,

$$V^*((i-1)\delta) = V^*(i\delta) - \text{tr}(\dot{\tilde{\Gamma}}(i\delta)V^*(i\delta)^\top)\Gamma(i\delta)\delta + A(i\delta)\Gamma(i\delta)\delta, \quad (15)$$

where  $A(i\delta)$  is updated at each step using (12). Unfortunately,  $V^*((i-1)\delta)$  obtained in this way is generally neither tangent to  $\mathcal{S}_m^k$  nor horizontal. Hence, this requires finding, at each step, the re-normalized horizontal component of  $V^*((i-1)\delta)$ . That is, at each step, we need to project  $V^*((i-1)\delta)$  to  $\tau_{\Gamma((i-1)\delta)}(\mathcal{S}_m^k)$  and then to the horizontal subtangent space of  $\mathcal{S}_m^k$  at  $\Gamma((i-1)\delta)$ , followed by normalizing it so that its length remains equal to that of  $V(s_0)$ .

Now, if  $X$  is a pre-shape matrix with  $\text{rank}(X) \geq m - 1$ , the projection of  $V \in M(m, k - 1)$  onto the tangent space  $\tau_X(\mathcal{S}_m^k)$  is given by

$$V_t = V - \text{tr}(VX^\top)X. \quad (16)$$

To obtain the projection of  $V_t \in \tau_X(\mathcal{S}_m^k)$  onto  $\mathcal{H}_X(\mathcal{S}_m^k)$ , we note that the orthogonal complementary subspace to  $\mathcal{H}_X(\mathcal{S}_m^k)$  in  $\tau_X(\mathcal{S}_m^k)$  is  $\mathcal{V}_X = \{AX \mid A = -A^\top\}$ . Since  $\{A_{ij} \mid 1 \leq i < j \leq m\}$  forms an orthonormal basis for the space of  $m \times m$

skew-symmetric matrices where  $A_{ij} = \frac{1}{\sqrt{2}}\{E_{ij} - E_{ji}\}$  and  $E_{ij}$  is the  $m \times m$  square matrix with all its elements zero except for the  $(i, j)$ th element which is one,  $\{A_{ij}X/\|A_{ij}X\| \mid 1 \leq i < j \leq m\}$  forms an orthonormal basis for  $\mathcal{V}_X$ . Thus, the projection of  $V_t \in \tau_X(\mathcal{S}_m^k)$  onto  $\mathcal{H}_X(\mathcal{S}_m^k)$  is given by

$$V_h = V_t - \sum_{1 \leq i < j \leq m} \frac{1}{\|A_{ij}X\|^2} \text{tr}(A_{ij}XV_t^\top) A_{ij}X. \quad (17)$$

Combining (15), (16) and (17), we have an approximation to  $\Psi_{\Gamma(s_0)}^{\Gamma((\ell-1)\delta)}(V(s_0))$  along the horizontal geodesic  $\Gamma(s)$ , after the first  $\delta$ -step, as

$$\Psi_{\Gamma((\ell-1)\delta)}^{\Gamma(s_0)}(V(s_0)) \approx \|V(s_0)\| \frac{W}{\|W\|} = V((\ell-1)\delta), \quad (18)$$

where  $W$  is obtained using (17) with  $V_t$  there replaced by

$$V^*((\ell-1)\delta) - \text{tr}(V^*((\ell-1)\delta)\Gamma((\ell-1)\delta)^\top)\Gamma((\ell-1)\delta) \quad (19)$$

and with  $X$  there replaced by  $\Gamma((\ell-1)\delta)$ , and where  $V^*((\ell-1)\delta)$  in (19) is obtained using (15). Note that (19) is the projection of  $V^*((\ell-1)\delta)$  to  $\tau_{\Gamma((\ell-1)\delta)}(\mathcal{S}_m^k)$  as given by (16). Recall that  $s_0 = \ell\delta$ . Then, since

$$\begin{aligned} \Psi_{\Gamma((\ell-2)\delta)}^{\Gamma(s_0)}(V(s_0)) &= \Psi_{\Gamma((\ell-2)\delta)}^{\Gamma((\ell-1)\delta)} \circ \Psi_{\Gamma((\ell-1)\delta)}^{\Gamma(s_0)}(V(s_0)) \\ &\approx \Psi_{\Gamma((\ell-2)\delta)}^{\Gamma((\ell-1)\delta)}(V((\ell-1)\delta)), \end{aligned}$$

application of (18) with  $\ell$  replaced by  $\ell-1$  again gives us an approximation to  $\Psi_{\Gamma((\ell-2)\delta)}^{\Gamma(s_0)}(V(s_0))$ . Finally, repeating this backward induction on  $\ell$  will result in an approximation to  $\Psi_{\Gamma(0)}^{\Gamma(s_0)}(V(s_0))$ . A similar procedure forward on  $\ell$  will give an approximation to  $\Psi_{\Gamma(s_0)}^{\Gamma(0)}(V(0))$ .

### 3.3 Shape spline fitting algorithm

We are now in a position to construct an algorithm to calculate the shape-space spline, or simply the shape spline, for a given set of configurations in  $\mathbb{R}^m$ , observed at times  $t_0, \dots, t_n$ , whose pre-shapes are denoted by  $X_0, \dots, X_n$ , in a similar fashion to that given in Kume et al. (2007), as follows.

**Algorithm 3.1.** *Let  $\delta$  and  $\varepsilon$  be two given small positive numbers.*

1. Rotate the successive pre-shapes,  $X_{i+1}$ , such that the resulting  $X_{i+1}$  is the Procrustes fit of the original one onto  $X_i$ . That is, rotate the successive pre-shapes  $X_{i+1}$  to satisfy the conditions that  $X_iX_{i+1}^\top$  is symmetric and that all its eigenvalues are non-negative except possibly for the smallest one whose sign is the same as the sign of  $\det(X_iX_{i+1}^\top)$ . Denote the set of the resulting pre-shapes by  $\mathcal{D} = \{X_i : 0 \leq i \leq n\}$  and let  $\Gamma_{\mathcal{D}}$  be the initial piecewise horizontal geodesic of  $\mathcal{D}$  such that  $\Gamma_{\mathcal{D}}(t_i) = X_i$ .

2. Construct  $G$  grid points between successive two times such that

$$t_0 = t_{00} < t_{01} < t_{02} < \dots < t_{0G} < t_1 = t_{10} < \dots < t_{ij} < \dots < t_n = t_{n0}$$

which gives  $t_{ij}, i = 0, 1, \dots, n, j = 0, 1, \dots, G$  for  $i \leq n - 1$  and  $j = 0$  for  $i = n$  where the difference between successive  $t_{ij}$  is less than or equal to  $\delta$ .

3. Set the base path  $\Gamma_{\mathcal{D}_1}$  to be the piecewise horizontal geodesic passing through  $\mathcal{D}_1 = \{\Gamma_{\mathcal{D}}(t_{ij}) : \forall i, j\}$ .
4. Using the unrolling and unwrapping procedures described in the previous section, with the parallel transport  $P$  there replaced by  $\Psi$  defined by (10), using the expression (6) for the inverse exponential, and using the approximation procedure for  $\Psi$  described at the end of the previous subsection, unwrap the data  $\mathcal{D}$  into  $\tau_{\Gamma_{\mathcal{D}_1}(t_0)}(\mathcal{S}_m^k)$  with respect to the base path  $\Gamma_{\mathcal{D}_1}$  which gives

$$\mathcal{D}^\dagger := \{X_0^\dagger, X_1^\dagger, \dots, X_n^\dagger\} \subset \mathcal{H}_{\Gamma_{\mathcal{D}_1}(t_0)}(\mathcal{S}_m^k).$$

5. Fit the cubic smoothing spline (1) to  $\mathcal{D}^\dagger$  and find fitted values at the times of the grid points given in Step 2, giving

$$\mathcal{D}_2^\dagger := \{Z_{ij}^\dagger = \widehat{f}^\dagger(t_{ij}, \hat{\lambda}) : i, j\} \subset \mathcal{H}_{\Gamma_{\mathcal{D}_1}(t_0)}(\mathcal{S}_m^k).$$

6. Using the wrapping procedure described in the previous section with the parallel transport  $P$  there replaced by  $\Psi$  defined by (10), using (4) for the exponential map on the sphere  $\mathcal{S}_m^k$ , and using the approximation procedure for  $\Psi$  described at the end of the previous subsection, wrap  $\mathcal{D}_2^\dagger$  back into the pre-shape sphere with respect to the base path  $\Gamma_{\mathcal{D}_1}$ , giving  $\mathcal{D}_2 := \{Z_{ij} : i, j\} \subset \mathcal{S}_m^k$ .
7. Successively rotate  $Z_{ij}$  in  $\mathcal{D}_2$  such that the resulting  $Z_{i,j+1}$  is the Procrustes fit of the original one onto  $Z_{ij}$ , and obtain the piecewise horizontal geodesic  $\Gamma_{\mathcal{D}_2}$  passing through the resulting  $Z_{ij}$ . Then,  $\Gamma_{\mathcal{D}_2}$  becomes the base path in the next iteration.
8. If  $\max\{d([\Gamma_{\mathcal{D}_2}(t_{ij})], [\Gamma_{\mathcal{D}_1}(t_{ij})]) : i, j\} \geq \varepsilon$ , replace  $\mathcal{D}_1$  by  $\mathcal{D}_2$  (where  $d$  is the shape distance); successively rotate  $X_i$  in  $\mathcal{D}$  such that the resulting  $X_i$  is the Procrustes fit of the original one onto  $Z_{i0}$ ; update  $\mathcal{D}$  by the resulting  $X_i$ ; and then go to Step 4. Otherwise, stop the iterations.

The linear spline is fitted to the data using the same iterative algorithm except that in step 5 we fit the linear spline (2) rather than the cubic smoothing spline (1). Also, for the single geodesic case ( $\lambda \rightarrow \infty$ ) again the same iterative algorithm is used.

### 3.4 Size-and-shape splines

All these results have analogues in the size-and-shape setting, where we do not have invariance under scaling. For example, for a configuration in  $\mathbb{R}^m$  with  $k(> m)$  labelled landmarks, its pre-size-and-shape is what is left after the effects of translation are removed. This pre-size-and-shape can be represented by an  $m \times (k-1)$  matrix  $\tilde{X} \in M(m, k-1)$  and the space of the pre-size-and-shapes,  $\mathcal{SS}_m^k$ , is identical with  $M(m, k-1)$ . For  $\tilde{X} \neq 0$ , the tangent space  $\tau_{\tilde{X}}(\mathcal{SS}_m^k)$  is then also  $M(m, k-1)$  and the horizontal subspace of  $\tau_{\tilde{X}}(\mathcal{SS}_m^k)$ , with respect to the quotient map from  $\mathcal{SS}_m^k$  to the Kendall size-and-shape space  $S\Sigma_m^k$ , is given by

$$\mathcal{H}_{\tilde{X}}(\mathcal{SS}_m^k) = \{V \in M(m, k-1) \mid \tilde{X}V^\top \text{ is symmetric}\}.$$

Horizontal geodesics in  $\mathcal{SS}_m^k$  starting from  $\tilde{X}$  take the form

$$\tilde{\Gamma}(s) = \tilde{X} + sV,$$

where  $V \in \mathcal{H}_{\tilde{X}}(\mathcal{SS}_m^k)$ . For two given size-and-shapes  $[\tilde{X}_1]$  and  $[\tilde{X}_2]$ , let  $\tilde{X}_1$  and  $\tilde{X}_2$  be the pre-size-and-shapes of  $[\tilde{X}_1]$  and  $[\tilde{X}_2]$  respectively such that  $\tilde{X}_1\tilde{X}_2^\top$  is symmetric and all its eigenvalues are non-negative except possibly for  $\lambda_m$ , the smallest one, where  $\text{sign}(\lambda_m) = \text{sign}(\det(\tilde{X}_1\tilde{X}_2^\top))$ . Then,  $\tilde{X}_2 - \tilde{X}_1 \in \mathcal{H}_{\tilde{X}}(\mathcal{SS}_m^k)$  and a shortest geodesic from  $[\tilde{X}_1]$  to  $[\tilde{X}_2]$  can be represented by the horizontal geodesic that connects  $\tilde{X}_1$  and  $\tilde{X}_2$ :

$$\tilde{\Gamma}(s) = \tilde{X}_1 + s(\tilde{X}_2 - \tilde{X}_1), \quad s \in [0, 1]. \quad (20)$$

Thus, the inverse exponential map  $\exp_{[\tilde{X}_1]}^{-1}([\tilde{X}_2])$  on the size-and-shape space  $S\Sigma_m^k$ , using its horizontal lift on  $\mathcal{SS}_m^k$ , is isometrically represented by

$$\exp_{\tilde{X}_1}^{-1}(\tilde{X}_2) = \tilde{X}_2 - \tilde{X}_1,$$

as long as the geodesic between  $[\tilde{X}_1]$  and  $[\tilde{X}_2]$  is unique.

Moreover, a modification of the argument given in [Le \(2003\)](#) shows that, along a horizontal size-and-shape geodesic  $\tilde{\Gamma}(s)$  in  $\mathcal{SS}_m^k$ , the vector field  $V(s)$  is horizontal and its projection to  $\tau_{[\tilde{\Gamma}(s)]}(S\Sigma_m^k)$  is the parallel translation, along the size-and-shape geodesic  $[\tilde{\Gamma}(s)]$ , of the projection of  $V(0)$  onto  $\tau_{[\tilde{\Gamma}(0)]}(S\Sigma_m^k)$  if and only if  $V(s)$  satisfies the conditions [\(8\)](#) and

$$\dot{V}(s) = A(s)\tilde{\Gamma}(s) \quad \text{for some } A(s) \text{ such that } A(s) = -A(s)^\top.$$

Thus, it follows from the proof for [Proposition 3.1](#) that the result of [Proposition 3.1](#) can also be generalized to size-and-shape space.

**Corollary 3.1.** *Let  $\tilde{\Gamma}(s)$ ,  $0 \leq s \leq s_0$ , be a given horizontal  $\mathcal{C}^1$ -curve in  $\mathcal{SS}_m^k$  and  $V$  be a given horizontal tangent vector in  $\tau_{\tilde{\Gamma}(0)}(\mathcal{SS}_m^k)$ . Assume that  $\text{rank}(\tilde{\Gamma}(s)) \geq m-1$ , except for at most finitely many  $s$ . Then, the vector field  $V(s)$  along  $\tilde{\Gamma}(s)$*

is horizontal and the projection of  $V(s)$  to  $\tau_{[\tilde{\Gamma}(s)]}(S\Sigma_m^k)$  is the parallel transport, along the size-and-shape curve  $[\tilde{\Gamma}(s)]$ , of the projection of  $V$  onto  $\tau_{[\tilde{\Gamma}(0)]}(S\Sigma_m^k)$  if and only if  $V(s)$  is the solution of

$$\begin{aligned}\dot{V}(s) &= A(s)\tilde{\Gamma}(s), & s \in [0, s_0], \\ V(0) &= V,\end{aligned}$$

where  $A(s)$  is skew-symmetric and is the unique solution to (12) with  $\Gamma$  being replaced by  $\tilde{\Gamma}$ .

A practical alternative to working directly in size-and-shape space is to work with independent splines in the product of the univariate centroid size space ( $\mathbb{R}^+$ ) and shape space ( $\Sigma_m^k$ ). In many practical applications it can be helpful to separate size and shape in this manner, so that size does not overly dominate the statistical analysis.

## 4 Applications

In this section, we illustrate our proposed method by applying it to simulated data as well as to real data. For notational convenience we designate the starting index by 1 instead of 0, i.e. the  $n$  data points are measured at times  $t_1, \dots, t_n$ .

Our simulation and real data analyses have been implemented in R (R Development Core Team, 2019). The function `smooth.spline` was used for fitting the cubic smoothing splines, the function `elspline` in the package `lspline` was used for fitting linear splines, and the package `shapes` was used for the Procrustes analysis and the relevant shape functions (Dryden, 2018). We used  $G = 2$  interpolation points between each pair of data points for a smooth base path and we chose  $\varepsilon = 10^{-5}$  for the convergence in the fitting algorithm for the simulated data and  $\varepsilon = 10^{-3}$  for the peptide data. The choice of the smoothing parameter  $\lambda$ , adapted to the data, is determined by applying the (Euclidean) leave-one-out cross-validation method (Efron and Tibshirani (1993), Chapter 17) to the unrolled shape spline and the unwrapped shape data. That is, we chose the optimal  $\lambda$  which minimizes

$$CV(\lambda) = \frac{1}{n} \sum_{i=1}^n \left\| v_i - \widehat{f_{\lambda, -i}^\dagger}(t_i) \right\|^2,$$

where  $\widehat{f_{\lambda, -i}^\dagger}$  is the unrolling of  $\widehat{f_{\lambda, -i}}$  to the tangent space at its starting point,  $\widehat{f_{\lambda, -i}}$  is the smoothing shape spline with the  $i$ th observation excluded and  $v_i$  is the unwrapped  $i$ th observed shape data with respect to  $\widehat{f_{\lambda, -i}}$ . The candidates for  $\lambda$  in the cross-validation were taken from the set  $\{10^{-9}, 10^{-7}, 10^{-5}, 10^{-3}, 10^{-1}\}$  for the simulation study and we also included  $10^{-6}, 10^{-4}$  for the peptides. Consequently in the following applications the chosen smoothing parameters for the original and perturbed data in the simulation study are  $\lambda = 10^{-5}$  and  $\lambda = 10^{-3}$ , respectively, and for the peptide data analysis we have  $\lambda = 10^{-4}$ .

## 4.1 Simulation

We consider configurations in  $\mathbb{R}^3$  with  $k = 8$  landmarks. Four initial vertex configurations are chosen such that the Riemannian shape distances between successive configurations are 0.47, 0.75 and 0.54 respectively. Note that the Riemannian shape distance ranges over  $[0, \pi/2]$ , so that the shapes of these consecutive configurations are not relatively close. Then four equally spaced shapes on each of the three geodesic segments connecting the successive shapes of the vertex configurations are generated; the configurations of these 16 shapes are shown in Figure 2, where the 1st, 6th, 11th and 16th are the four initial configurations. Then, we add Gaussian noise with standard deviation  $\sigma = 0.05$  independently to each landmark of the original configurations to generate perturbed data which is shown in Figure 3.

Figure 4 shows the configurations of the fitted shapes on the smoothing shape spline to the perturbed data.

To visualize the fitted smoothing shape splines to the original and perturbed data respectively, in each case we unroll the given 16 shapes onto the base tangent space to the first shape along the piecewise geodesic segments through them and unroll the fitted smoothing shape spline onto the tangent space to its starting point. Then, we carry out the principal component analysis on the coordinates of these four unrolled data sets respectively. Figure 5 shows the first two principal component scores of the unrolled original data and the corresponding fitted shape spline, in (a), and the unrolled perturbed data ( $\sigma = 0.05$ ) and the corresponding fitted shape spline, in (b). The given data are displayed as squares and the dotted lines are for the fitted shape spline with ‘s’ indicating the starting point. For the original non-perturbed data set, the proportion of variance explained by PC1 and PC2 is 78.4% and 15.4% respectively and, for the fitted shape spline to the perturbed data, 59.7% and 15.7% are explained by PC1 and PC2. Although path of the configurations lies close to a plane, it is not exactly in a plane. For the original data the percentage of variability in the first two tangent space PCs is 93.8%, and so the remainder of the variability is in the third PC (6.2%) which is small and so we ignore this dimension in our analysis.

Noting that the two turning points of these three geodesic segments are at the 6th and 11th configurations, Figure 5(a) clearly shows the structure of the three geodesic segments which is in accord with the simulation setting. For the perturbed data set, the overall pattern is similar to that of the original data but with local differences due to the noise.

Further examples are also given in Figure 6 with different independent Gaussian noise levels (a)  $\sigma = 0.02$ , (b)  $\sigma = 0.1$ , and independent Student’s  $t_3$  noise with standard deviation (c)  $\sigma = 0.02$  and (d)  $\sigma = 0.05$ . In the cases (a)-(c) the three segments can be seen in the fitted paths. The final plot (d) contains a large outlier and the structure is harder to see. Note that with more noise in (b) and (d) the first two PCs explain a smaller percentage of the shape variability (57.5% and 71.2% respectively for (b) and (d)).

Routines are available in R ([R Development Core Team, 2019](#)) at

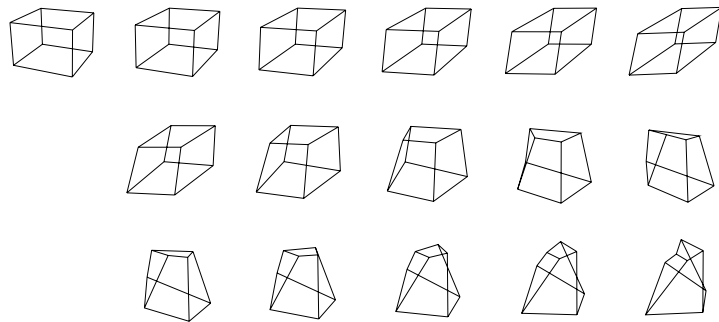


Figure 2: Original configurations.

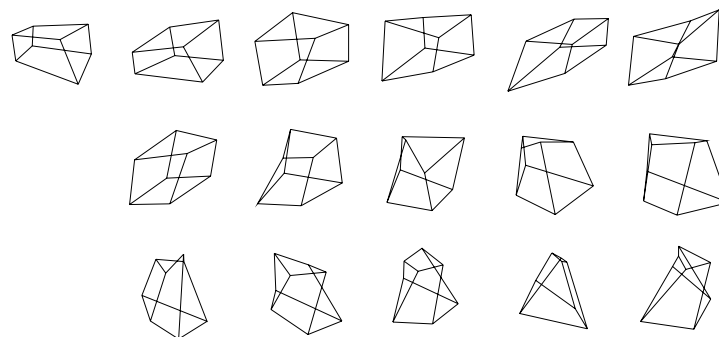


Figure 3: Perturbed configurations.

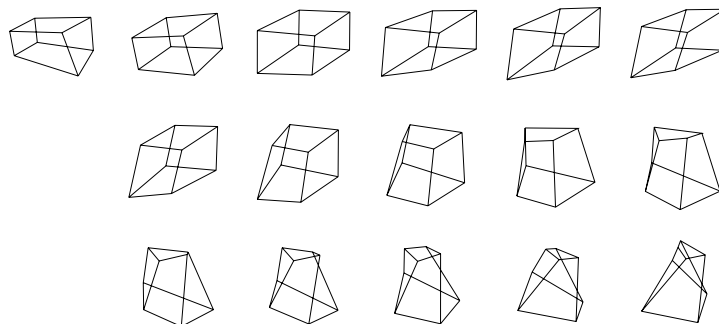


Figure 4: Configurations of the fitted shapes to the shapes of the perturbed configuration data.

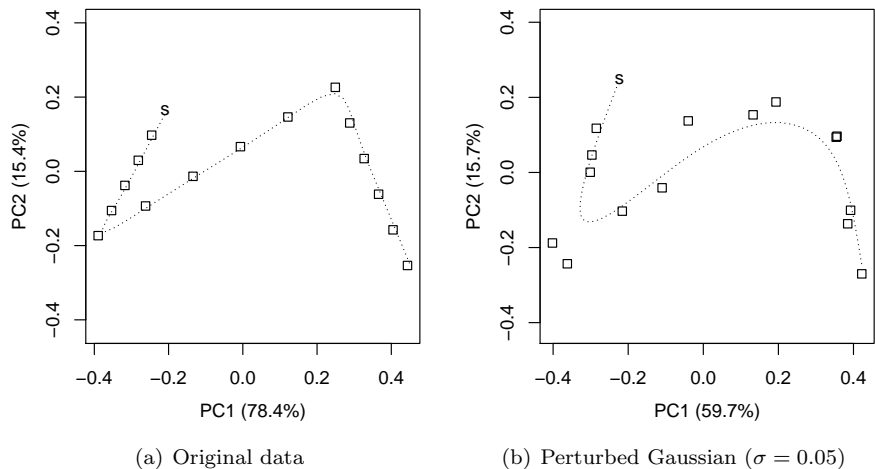
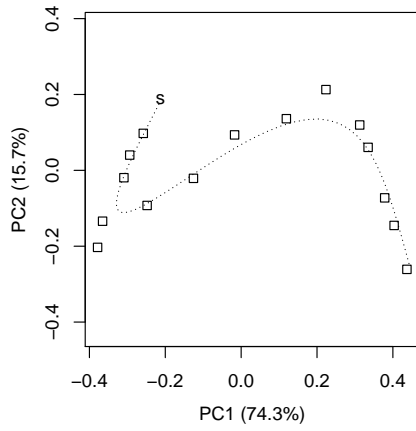


Figure 5: The first two principal component scores of the unrolled shape data and unrolled fitted shape spline in the tangent spaces at the starting points.

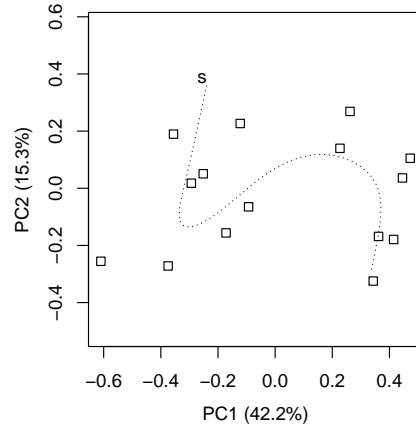
<https://www.maths.nottingham.ac.uk/plp/pmezild/papers/splines3D>  
to compute smoothing splines and reproduce all the examples of the paper. The algorithm is computationally intensive and, for example, fitting the spline using cross validation to obtain  $\lambda$  followed by the chosen  $\lambda$  fit with  $G = 2$  interpolated points for the  $\sigma = 0.05$  Gaussian simulated data takes 3.16 minutes in total. In all our examples the spline fitting algorithm converges for the  $\lambda$  chosen by cross-validation. However, the algorithm may not converge on some occasions, particularly if an inappropriate choice of  $\lambda$  is made, and so setting an upper limit on the number of iterations (e.g. 20) is helpful in practice.

## 4.2 Peptide data

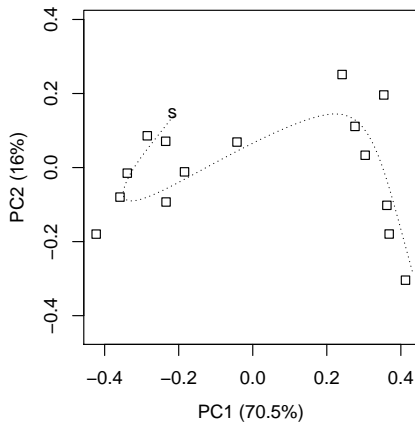
In molecular biology, it is of great interest to study the changes in shape of a protein, as shape is an important component of a protein's function. Studies of this type are often approached through molecular dynamics simulations, which are large deterministic simulations using Newtonian mechanics to model the movement of a protein in a box of water molecules (e.g. [Salomon-Ferrer et al., 2013](#)). We consider a dataset of in the study of the small alanine pentapeptide (Ala<sub>5</sub>) which consists of  $k = 29$  atoms in  $\mathbb{R}^3$  at 10000 equal picosecond ( $10^{-12}s$ ) time intervals. The data were provided by Professor Charles Laughton, School of Pharmacy, University of Nottingham, and further detail on this particular peptide is given by [Margulis et al. \(2002\)](#) and [Dryden et al. \(2019\)](#). In particular from [Dryden et al. \(2019\)](#) there are four clusters (preferred states) of the peptide shape, and it is of interest to describe the shapes of the clusters and the predicted transitions between the states.



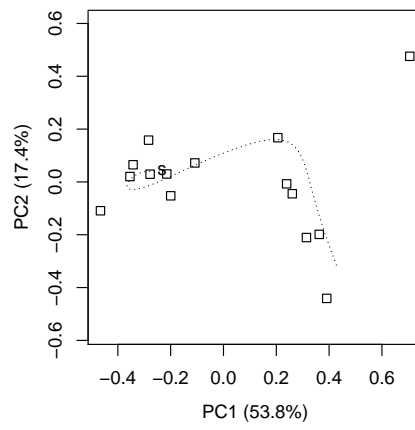
(a) Perturbed Gaussian ( $\sigma = 0.02$ )



(b) Perturbed Gaussian ( $\sigma = 0.1$ )



(c) Perturbed  $t_3$  ( $\sigma = 0.02$ )



(d) Perturbed  $t_3$  ( $\sigma = 0.05$ )

Figure 6: The first two principal component scores of the unrolled shape data and unrolled fitted shape spline in the tangent spaces at the starting points for independent (a) Gaussian noise levels (a)  $\sigma = 0.02$ , (b)  $\sigma = 0.1$ , and independent Student's  $t_3$  noise with standard deviation (c)  $\sigma = 0.02$  and (d)  $\sigma = 0.05$

We apply the smoothing shape spline fitting to a small temporal subsequence of 30 configurations equally spaced in time, spanning a 10 nanosecond ( $10^{-8}s$ ) period, and we consider several different models. Planar projections of these configurations are presented in Figure 7 as rainbow coloured dots where red and violet points indicate the first and last landmarks, respectively. The peptide configuration at the start of this sequence is very irregular in all three dimensions at  $t = 1$ , then it gradually straightens over time so that we see a more smoothly curved form at  $t = 30$ . Their shapes vary substantially with largest pairwise Riemannian shape distance 1.028 (where the maximum possible value is  $\pi/2$ ) and this motivates us to consider analysis based on unrolling and unwrapping to a base tangent space, rather than the more straightforward analysis based on a single tangent space projection.

In Figure 7 the fitted configurations to the moving configurations are indicated by ‘x’ with connecting solid lines, and  $\lambda = 10^{-4}$  is the smoothing parameter chosen by cross-validation.

We also compare some alternative models including a single geodesic model and linear splines in the base tangent space with 3, 4, 5, 6, 7 equally spaced knots. We assume an independent Gaussian model for errors in the base tangent space with variance  $\sigma_i^2$  in the  $i$ th tangent space dimensions,  $i = 1, \dots, M = 87 - 7 = 80$ . The total number of parameters  $p$  in each model is given in Table 1, although for the cubic spline we use the sum of the effective degrees of freedom plus the number of variance parameters. For the information criteria we use

$$IC = n \sum_i \log \hat{\sigma}_i^2 + K_{IC} p$$

where  $K_{IC} = 2$  for the Akaike Information Criterion (AIC) and  $K_{IC} = \log n$  for the Bayesian Information Criterion (BIC), and preferred models have smaller ICs. Here the sample size  $n$  is not large compared to  $p$  and so we use these criteria as informal guides rather than for formal model choice.

Model	$\sum_i \log(\hat{\sigma}_i^2)$	$p$	AIC	BIC
Geodesic	-259.5	240	-7305	-6969
Linear spline 3 knots	-270.5	320	-7476	-7028
Linear spline 4 knots	-297.7	400	-8130	<b>-7570</b>
Linear spline 5 knots	-297.9	480	-7977	-7304
Linear spline 6 knots	-311.8	560	-8235	-7450
Linear spline 7 knots	-321.3	640	-8360	-7463
Cubic spline 31 knots	-349.4	871.7*	<b>-8739</b>	-7518

Table 1: Model fitting and comparison using AIC and BIC. \*Using effective degrees of freedom plus number of variance parameters.

We can see that the linear spline with 4 knots and the cubic spline are favoured using BIC and AIC respectively, and with BIC there is little to choose between the linear 4 knots model and the cubic spline model. This can also be

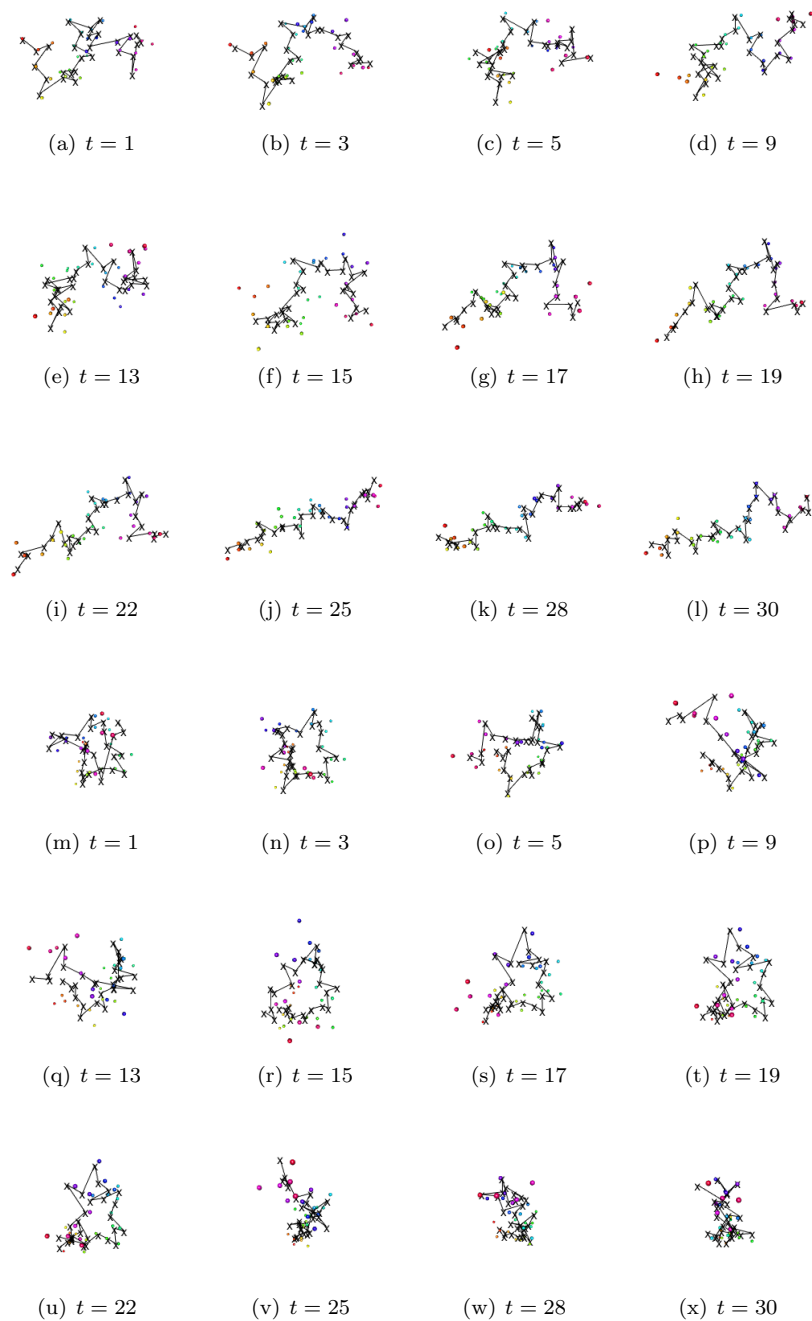


Figure 7: Configurations of a dynamic short peptide. In each subfigure, rainbow coloured dots indicate 29 landmarks and the connected points 'x' are the fitted configurations. One particular view is given in (a)-(l) and an orthogonal view is given in (m)-(x).

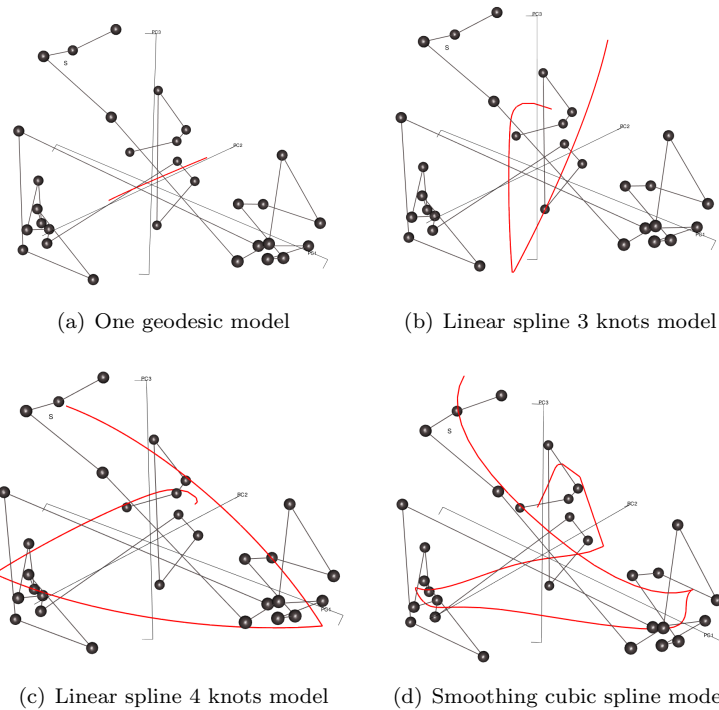


Figure 8: Principal component scores. Dots are at data points and the solid thick lines are at fitted values. ('S' is located near to the starting point.)

seen in Figure 8 which shows the first three shape principal component scores of the 30 peptide configurations in the Procrustean tangent space at their mean shape. PC scores 1,2,3 explain 43.1%, 22.0% and 12.3% of the shape variability respectfully, and so this includes the most important aspects of shape variability. The connected dots indicate the PC scores of the data points and the red lines on the other hand are the PC scores of the fitted paths, where their approximate starting points are indicated by ‘S’ in all panels. The curved PC score curves in (b) and (c) are as expected as the mean shape of these peptides does not lie in either of these fitted geodesic segments. As shown in (a), (b), the geodesic and linear spline 3 knots models do not explain the data points well. On the other hand, the (c), (d) the linear spline 4 knots model and cubic spline model are more reasonable. Both (c) and (d) provide a fit to each of the four clusters of shapes in the data with transition paths inbetween. These four clusters have been observed in this dataset in earlier studies (Dryden et al., 2019).

If we had used the Procrustes tangent space at the outset for spline fitting there would have been distortions in the distances between neighbouring configurations, particularly near the end of the sequence, leading to inaccurate predictions. In particular, the Procrustes tangent space distance between neighbouring pairs of configurations is around 20 – 75% larger than the Riemannian distance at times 24, 25, 26, 28, whereas it is within 10% for the rest of the sequence. In the most extreme case between  $t = 26$  to  $t = 27$  the Procrustes tangent distance is 0.648 whereas the Riemannian distance is 0.374, and we can see extra curvature in the fitted spline near the end of the sequence in the PC scores plot in Figure 8(d).

An attractive feature of the spline fit is that smooth paths between clusters can be explored, to investigate how a peptide transitions in shape from one cluster to another. In Figure 9 we display the predicted shape change in the transition to the final cluster using the cubic spline. For the smooth prediction we have used the data at all the integer times  $t = 1, \dots, 30$  but have predicted at a pair of equally spaced time points between integer times. We can see that the smooth path predicts the shape change between data points reasonably well, and that the straightening of the peptide is seen in the smoothed predicted path in shape space.

Although the two dimensional projections of some peptides in Figure 7 look close to collinearity, their actual three-dimensional figures are not close to collinearity. Hence, their shapes are not close to the singularity set. For example the 1st principal axis of the final peptide explains 90.5% of the variability, and while this is fairly high it is quite far from being collinear ( $\sim 100\%$ ).

We have chosen to remove size for the peptides and concentrate on shape information alone. The centroid size of the peptide is given in Figure 10 and we see that the final part of the sequence is a little larger according to this measure. If scale is important to retain than a reasonable approach could be to consider a product of a univariate cubic/linear spline on the scalar centroid size with our spline on the shape space.

Note finally that there are many other applications of smoothing splines on Riemannian manifolds (e.g., see Su et al., 2012). The main advantage of

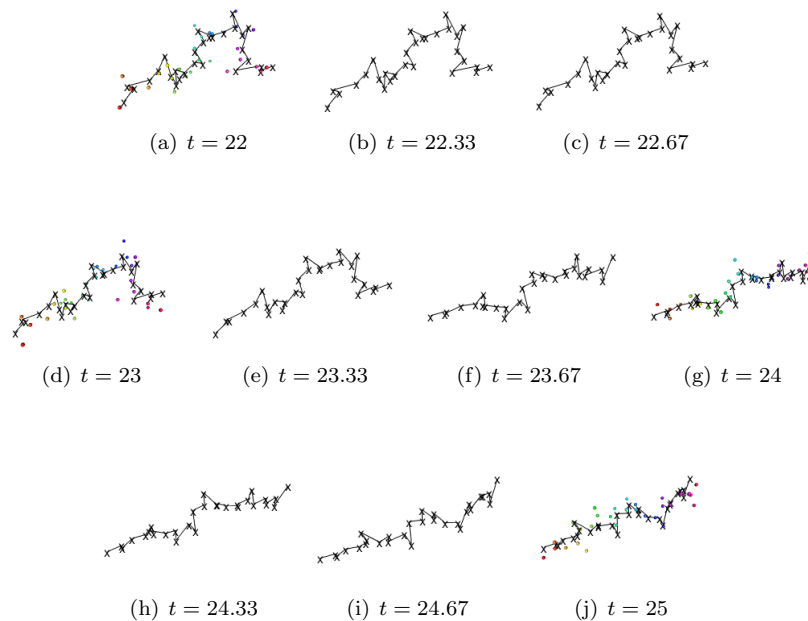


Figure 9: Configurations of a moving short peptide and predictions for part of the sequence using the cubic spline. The rainbow coloured dots indicate 29 landmarks and the connected points 'x' are the fitted configurations. Every integer time point has been used for the spline fitting, and the predictions are shown inbetween (at non-integer time points)

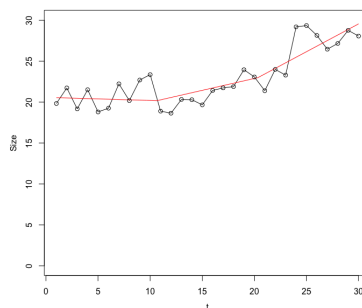


Figure 10: Centroid size for the peptide data (black), and a fitted linear spline with 4 knots (in red).

the unwrapping and unrolling method over a simple tangent space method is that much larger variations in data can be handled, such as are present in the peptide application. Since it is possible to bypass the need for the knowledge of the curvature tensor in the unrolling technique as demonstrated in [Su et al. \(2012\)](#), our implementation of spline fitting on manifolds does not involve the curvature tensor explicitly. In this sense, unlike some alternative spline methods in [Su et al. \(2012\)](#), we do not need to know the complete geometrical structure of the manifold, and hence the range of potential applications is very broad indeed.

## Acknowledgement

This work was supported by the Engineering and Physical Sciences Research Council grant number EP/K022547/1 and Royal Society Wolfson Research Merit Award WM110140.

## References

- Cornea, E., Zhu, H., Kim, P., and Ibrahim, J. G. (2017). Regression models on Riemannian symmetric spaces. *J. R. Stat. Soc. Ser. B. Stat. Methodol.*, 79(2):463–482.
- Dryden, I. L. (2018). *Shapes: Statistical Shape Analysis*. R package version 1.2.4.
- Dryden, I. L., Kim, K.-R., Laughton, C. A., and Le, H. (2019). Principal nested shape space analysis of molecular dynamics data. *arXiv e-prints*, page arXiv:1903.09445.
- Dryden, I. L. and Mardia, K. V. (2016). *Statistical Shape Analysis, with Applications in R, 2nd edition*. Wiley, Chichester.
- Efron, B. and Tibshirani, R. (1993). *An Introduction to the Bootstrap*. Chapman and Hall, London.
- Fletcher, P. T. (2013). Geodesic regression and the theory of least squares on Riemannian manifolds. *Int. J. Comput. Vis.*, 105(2):171–185.
- Fletcher, P. T., Lu, C., Pizer, S. M., and Joshi, S. (2004). Principal geodesic analysis for the study of nonlinear statistics of shape. *IEEE Transactions on Medical Imaging*, 23:995–1005.
- Green, P. J. and Silverman, B. W. (1994). *Nonparametric Regression and Generalized Linear Models: A Roughness Penalty Approach*. Chapman and Hall, London.
- Hinkle, J., Fletcher, P. T., and Joshi, S. (2014). Intrinsic polynomials for regression on Riemannian manifolds. *J. Math. Imaging Vision*, 50(1-2):32–52.

- Huckemann, S., Hotz, T., and Munk, A. (2010). Intrinsic shape analysis: geodesic PCA for Riemannian manifolds modulo isometric Lie group actions. *Statist. Sinica*, 20(1):1–58.
- Huckemann, S. and Ziezold, H. (2006). Principal component analysis for riemannian manifolds, with an application to triangular shape spaces. *Adv. Appl. Prob.*, 38:299–319.
- Jupp, P. E. and Kent, J. T. (1987). Fitting smooth path to spherical data. *Appl. Statist.*, 36:34–46.
- Kendall, D. G. (1984). Shape manifolds, Procrustean metrics and complex projective spaces. *Bulletin of the London Mathematical Society*, 16:81–121.
- Kendall, D. G., Barden, D., Carne, T. K., and Le, H. (1999). *Shape and Shape Theory*. Wiley, Chichester.
- Kenobi, K., Dryden, I. L., and Le, H. (2010). Shape curves and geodesic modelling. *Biometrika*, 97:567–584.
- Kent, J. T. and Mardia, K. (2001). Shape, Procrustes tangent projections and bilateral symmetry. *Biometrika*, 88:469–485.
- Kent, J. T., Mardia, K. V., Morris, R. J., and Aykroyd, R. G. (2001). Functional models of growth for landmark data. In *In Proceedings in Functional and Spatial Data Analysis*, pages 109–115. Leeds: University of Leeds Press. LASR2001, Ed. K. V. Mardia and R. G. Aykroyd.
- Koenker, R. and Mizera, I. (2004). Penalized triograms: total variation regularization for bivariate smoothing. *Journal of the Royal Statistical Society: Series B (Statistical Methodology)*, 66(1):145–163.
- Kume, A., Dryden, I. L., and Le, H. (2007). Shape-space smoothing splines for planar landmark data. *Biometrika*, 94:513–528.
- Le, H. (2003). Unrolling shape curves. *J. Lond. Math. Soc.*, 68:511–526.
- Le, H. and Kume, A. (2000). Detection of shape changes in biological features. *Journal of Microscopy*, 200:140–147.
- Lin, L., St. Thomas, B., Zhu, H., and Dunson, D. B. (2017). Extrinsic Local Regression on Manifold-Valued Data. *J. Amer. Statist. Assoc.*, 112(519):1261–1273.
- Margulis, C. J., Stern, H. A., and Berne, B. J. (2002). Helix unfolding and intramolecular hydrogen bond dynamics in small  $\alpha$ -helices in explicit solvent. *J. Phys. Chem. B*, 106:10748–10752.

- Morris, R. J., Kent, J. T., Mardia, K. V., Fidrich, M., Aykroyd, R. G., and Linney, A. (1999). Analysing growth in faces. In *In Proceedings of the International Conference on Imaging Science, Systems and Technology, Las Vegas, 1999*, Ed. H. R. Arabnia, pages 404–409. Bogart, GA: Computer Science Research, Education and Applications (CSREA) Press.
- Patrangenaru, V. and Ellingson, L. (2016). *Nonparametric statistics on manifolds and their applications to object data analysis*. CRC Press, Boca Raton, FL.
- Pauley, M. (2011). Jupp and Kent’s cubics in Lie groups. *J. Math. Phys.*, 52(1):013515, 9.
- Petersen, A. and Müller, H.-G. (2019). Fréchet regression for random objects with Euclidean predictors. *Ann. Statist.*, 47(2):691–719.
- R Development Core Team (2019). *R: A Language and Environment for Statistical Computing*. R Foundation for Statistical Computing, Vienna, Austria.
- Salomon-Ferrer, R., Case, D. A., and Walker, R. C. (2013). An overview of the Amber biomolecular simulation package. *Wiley Interdisciplinary Reviews: Computational Molecular Science*, 3(2):198–210.
- Srivastava, A. and Klassen, E. P. (2016). *Functional and Shape Data Analysis*. Springer, New York.
- Su, J., Dryden, I. L., Klassen, E., Le, H., and Srivastava, A. (2012). Fitting smoothing splines to time-indexed, noisy points on nonlinear manifolds. *Image and Vision Computing*, 30:428–442.
- Yuan, Y., Zhu, H., Styner, M., Gilmore, J. H., and Marron, J. S. (2013). Varying coefficient model for modeling diffusion tensors along white matter tracts. *Ann. Appl. Stat.*, 7(1):102–125.
- Zhu, H., Cheng, Y., Ibrahim, J. G., Li, Y., Hall, C., and Lin, W. (2009). Intrinsic regression models for positive-definite matrices with applications to diffusion tensor imaging. *Journal of the American Statistical Association*, 104:1203–1212.